Research Article

Xueping Du*, Zhijie Chen, Qi Meng, and Yang Song

Experimental analysis and ANN prediction on performances of finned oval-tube heat exchanger under different air inlet angles with limited experimental data

https://doi.org/10.1515/phys-2020-0212
received October 29, 2020; accepted November 07, 2020

Abstract: A high accuracy of experimental correlations on the heat transfer and flow friction is always expected to calculate the unknown cases according to the limited experimental data from a heat exchanger experiment. However, certain errors will occur during the data processing by the traditional methods to obtain the experimental correlations for the heat transfer and friction. A dimensionless experimental correlation equation including angles is proposed to make the correlation have a wide range of applicability. Then, the artificial neural networks (ANNs) are used to predict the heat transfer and flow friction performances of a finned oval-tube heat exchanger under four different air inlet angles with limited experimental data. The comparison results of ANN prediction with experimental correlations show that the errors from the ANN prediction are smaller than those from the classical correlations. The data of the four air inlet angles fitted separately have higher precisions than those fitted together. It is demonstrated that the ANN approach is more useful than experimental correlations to predict the heat transfer and flow resistance characteristics for unknown cases of heat exchangers. The results can provide theoretical support for the application of the ANN used in the finned oval-tube heat exchanger performance prediction.

Keywords: heat transfer, finned oval-tube heat exchanger, artificial neural network, air inlet angle, prediction

Nomenclature

a	length of the major axis/m
b	length of the minor axis/m
D_c	fin collar outside diameter/m
E	experimental data (output value)
f	flow friction factor
F_h	fin height/m
F_l	fin length/m
F_s	fin spacing/m
F_w	fin width/m
JF	JF factors, dimensionless
mse	mean squared error
n	number of samples
N_{tr}	number of tube rows
N_{tp}	number of tube-passes
Nu	Nusselt number
P	predicted value (target value)
P_l	longitudinal tube pitch/m
P_t	transverse tube pitch/m
R	linear regression coefficient
Re	Reynolds number
T	temperature/°C
θ	air inlet angles/°

1 Introduction

External finned tube heat exchangers are widely used in various industries such as chemical engineering and heating and ventilation compressor intercoolers. In particular, they occupy an extremely significant position in the air cooling towers and air separators. The extended surfaces on the air side are used effectively to enhance the heat transfer performance of such heat exchangers. The finned surface is a common type of extended surfaces. It can be used to destroy the boundary layer, increase the surface area, and change the flow pattern to meet the demand of heat transfer enhancement. The schematic diagram of the plain finned tube heat exchanger units is shown in Figure 1, including circular tubes, oval

* **Corresponding author: Xueping Du,** Department of Energy and Power Engineering, School of Electrical and Power Engineering, China University of Mining and Technology, Xuzhou 221116, People's Republic of China; Key Laboratory of Thermo-Fluid Science and Engineering (Xi'an Jiaotong University), Ministry of Education, Xi'an 710049, People's Republic of China,
e-mail: xpdcumt@cumt.edu.cn
Zhijie Chen, Qi Meng, Yang Song: Department of Energy and Power Engineering, School of Electrical and Power Engineering, China University of Mining and Technology, Xuzhou 221116, People's Republic of China

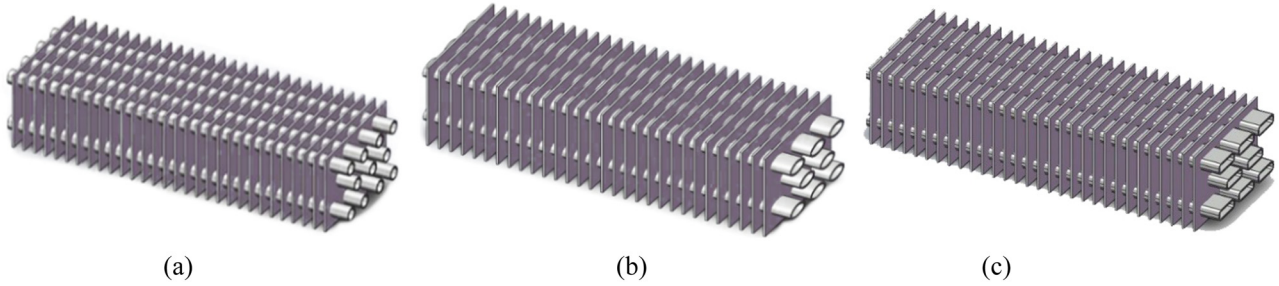

Figure 1: Schematic diagram of finned tube heat exchanger units: (a) circular tube, (b) oval tube, and (c) flat tube.

tubes, and flat tubes. As usual, the water or steam flows inside the tubes and the air flows across the finned tube bundles. Thus, the study on the flow and heat transfer performance of finned tube heat exchangers is very significant for the design and the optimization of heat exchangers. Much attention is paid on the experimental and numerical research of finned tube heat exchangers, and more useful results and correlations have been presented [1–5].

With the rapid development of artificial intelligence (AI) techniques, more intelligence algorithms are used successfully during the process of the optimal design of heat exchangers, such as artificial neural network (ANN) [6–10], evolution strategies (ES) and evolutionary programming (EP) [11], genetic algorithm (GA) [12–14], and particle swarm optimization (PSO) [15–18]. ANN has many attractive advantages. For example, ANN offers a new way to predict non-linear, uncertain, or unknown complex system without any explicit condition about input/output relationship. It can be applied to learn complex nonlinear relationship through certain network configuration and can be applied to simulate dynamically and control unknown or uncertain process [9].

Now ANN is widely used in various application areas such as function fitting, dynamic control, data clustering, pattern recognition, and system identification. In the thermal system, ANN is applied for performance prediction, heat transfer analysis, and dynamic control. For example, Yang and Sen [19,20] reviewed the work on dynamic modeling and controlling of heat exchangers using ANN and GA. Wang et al. [9,21,22] did much work on the performance prediction and analysis of the heat transfer and friction for heat exchangers through the ANN methods. Hosoz et al. [8] and Gao et al. [23] predicted the performances of cooling towers with ANN. Akbari et al. [24,25] predicted the steady state and the transient performance of a run-around membrane energy exchanger for yearly nonstop operation. Zdaniuk et al. [26] correlated the heat transfer and friction in helically finned tubes using ANNs, and it was concluded that ANNs were well suited for the application to helically finned tubes. Then, Zdaniuk et al. [27] made a comparison of ANNs with symbolic-regression-based correlations for optimization of helically finned tubes in heat exchangers. It was concluded that the predictive capability of the ANNs was superior to empirical correlations obtained by symbolic regression, when considering only their applicability to the available datasets, but much care must be exercised when using ANNs for optimization purposes to enhance the heat transfer. Mohanraj et al. [28] made a review about the applications of ANN for the energy analysis of refrigeration, air conditioning, and heat pump systems (RACHP). It was concluded that ANN could be successfully applied in the field of RACHP systems with acceptable accuracy. Besides, ANN is also used in the optimization of the HVAC system energy consumption in a building [29] and the type of the helical wire inserted tube in heat exchangers [30], and to predict thermal performances of the thermoelectric generator for the waste heat recovery [31] and the carbon nanotube nanofluid in a tube [32]. From the aforementioned successful applications of ANN in the thermal system, it can be seen that ANN is a significant tool for thermal analysis in the engineering system, especially in heat exchangers.

Furthermore, there is a widespread problem that the air inlet direction is not always perpendicular to the heat exchanger surface in many cases for the direct and indirect air cooling systems. The air oncoming flow direction has an important effect on the heat transfer and pressure drop performances of the air-cooled radiator. So the research and development of air inlet angles' influence on the air-side performances of heat exchangers have been paid more attention. Liu et al. [33] numerically studied the effect of the air inlet angles on the air-side performance of plate-fin heat exchangers in automotive radiators. Also the experiments were accomplished on finned oval-tube heat exchangers under four different air inlet angles in the author's previous studies [34–36].

After the experiment has been completed, a high accuracy of dimensionless correlations on the heat transfer and friction is always expected according to the limited experimental data. However, the experiment conditions are limited. So it needs to cost much energy to acquire more experiment data to improve the precision. Besides, during the procedure of reducing experimental data to get the experimental correlation for heat transfer and friction, certain errors are always generated by the traditional methods. Pacheco-Vega et al. [10] applied the ANN approach to accurately model thermal performances for the fin-tube refrigerating heat exchanger with limited experimental data, and the results showed that the ANN methodology gave an upper bound of the estimated error in the heat rates and the ANN procedure could also help the manufacturer to find where new measurements are needed. Peng and Ling [37] applied ANN to predict the thermal characteristics on plate-fin heat exchangers with limited experimental data. The predicted values were found to be in good agreement with the actual values from the experiments. However, they only researched on the effectiveness of ANN to predict thermal performances for fin-tube refrigerating heat exchangers and plate-fin heat exchangers with the limited experimental data, while few on the comparison of the predicted performances of ANN with those of experimental correlations of finned oval-tube heat exchangers and few on the difference between the heat transfer and flow characters predicted together and predicted separately.

In view of the aforementioned facts, this study proposes a dimensionless experimental correlation equation including air inlet angles to make the correlation have a wide range of applicability. It uses the air inlet angle divided by 90 degrees to make the angle dimensionless. Then, this study shows the procedure of an ANN fitting tool to predict the heat transfer and resistance performances on a finned oval-tube heat exchanger under four air inlet angles with the limited experimental data. Then, the performances of the results predicted by ANN are compared with those by experimental correlations. The results of Nu and f predicted separately are compared with those of Nu and f predicted together. Finally, the predicted performances when the data of the four air inlet angles are fitted separately are compared with those when they are fitted together to predict Nu and f. The results can provide the theoretical support for the application of the artificial intelligence in the heat exchanger performance prediction and optimization.

2 Physical model and experimental data

A finned oval-tube heat exchanger with two rows of tubes and single tube-pass under four different air inlet angles (90°, 60°, 45°, and 30°) was experimentally tested in the author's group [35]. The schematic view of the test finned oval-tube heat exchanger is shown in Figure 2, and the four air inlet angle (θ) is shown in Figure 3. To study the effect of the air inlet angle on the flow and heat transfer performance, the heat exchanger is arranged with an inclined angle in the experiment. The experimental system is shown in Figure 4.

During the experimental test, the hot water flows inside the oval tubes that are in staggered arrangement, while cold air flows across the finned oval-tube bundles, acting as a coolant. The heat is transferred from the hot water to the tube wall and then across the tube wall and finned surfaces to the cold air. The experiment was accomplished when the Reynolds number ranged from 1,300 to 13,000 on the air side. Sixty-three sets of experimental data were obtained for 90°, and 44 for 60°, 45 for 45°, and 45 for 30°. The experimental maximum uncertainties of the Nusselt number and the friction factor are 8.26% and 11.98%, respectively.

Because the convective heat transfer coefficient of the tube side can be calculated with Gnielinski correlation [38,39] and the thermal resistance of the heat-conductive part is known, the air-side convective heat transfer coefficient could be acquired through the thermal resistance separation methods. After the data reduction procedures, the experimental data have been fitted separately in logarithmic coordinates to acquire the classical experimental correlations of Nu versus Re and f versus Re under different

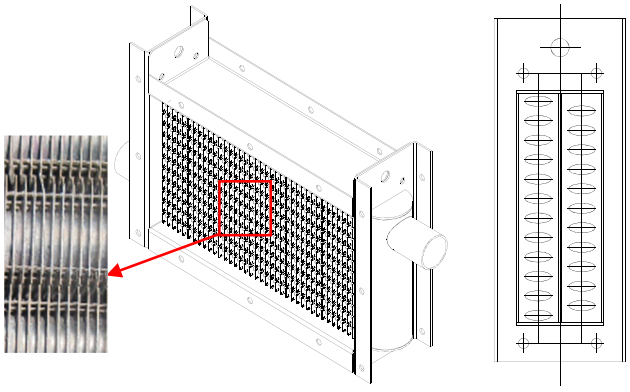

Figure 2: Schematic view of finned oval-tube heat exchanger.

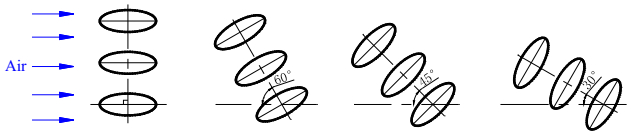

Figure 3: Four different air inlet angles (θ).

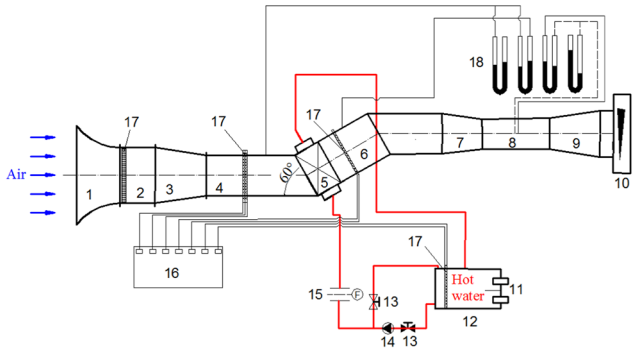

Figure 4: Schematic diagram of experimental system [35]. 1, Entrance; 2, transition section; 3, contraction section; 4, straightening section; 5, test section; 6, straightening section; 7, contraction section; 8, flow metering duct; 9, expansion section; 10, blower; 11, electric heating rod; 12, water tank; 13, valve; 14, water pump; 15, turbine flowmeter; 16, data acquisition system; 17, thermocouples grid; and 18, U tube manometer.

air inlet angles, which are presented in Table 1. The correlation coefficient (R) and standard deviation (SD) are used to quantify the generalization capacity. R and SD are described in detail in ref. [35].

In practice, there may be other angles between the heat exchanger and the inlet air, so to make the correlation have a wide range of applicability, a dimensionless experimental correlation equation including air inlet angles is proposed. The air inlet angles divided by 90 degrees are used to make the angle dimensionless. According to this form of fitting calculation, the dimensionless correlations with the air inlet angles are listed in equations (1) and (2). They could provide a theoretical support for related engineering applications

$$\mathrm{Nu} = 1.39\,\mathrm{Re}_{\mathrm{Dc}}^{0.46}\left(\frac{\theta}{90}\right)^{0.06}, \tag{1}$$

where the correlation coefficient (R) and standard deviation (SD) are 0.95 and 6.11, respectively.

$$f = \frac{69.26}{\mathrm{Re}_{\mathrm{Dc}}^{0.43}\left(\frac{\theta}{90}\right)^{0.006}}, \tag{2}$$

where the correlation coefficient (R) and standard deviation (SD) are 0.96, and 0.16, respectively. The angle ranges (θ) in the aforementioned two correlations is from 30° to 90°.

The comparisons of the experimental value with the value calculated from the experimental correlations including angles are shown in Figure 5. It can be seen that the experimental correlations for the Nusselt number has a relatively high accuracy, and 97% of the data are within the error line of 15%. However, 96% of the data are within the error line of 20% for the experimental correlation of the resistance coefficient.

To obtain the change law of the comprehensive heat transfer performance of the finned oval-tube heat exchanger at various angles, the JF factor [40] is used. JF is a dimensionless number that can effectively evaluate the thermal and dynamic performance of a heat exchanger since it includes both the j and the f factor. It is a larger-the-better characteristic, and its description is given in detail in ref. [40]. The JF factors of the finned oval-tube heat exchanger at the four air inlet angles are compared in Figure 6. Figure 6 shows when the Reynolds number is relatively small, the comprehensive performance at 60° is the best. While the Reynolds number is relatively large, the comprehensive performance at 45° is the best, and the critical Reynolds number is 6,685. The comprehensive performance at 30° is the worst. The reason may be that the air flow is disturbed, and the heat transfer is enhanced when the air flows into the heat exchanger obliquely at an angle. But when the air inlet angle is 30 degrees, the air flow resistance loss is too large, resulting in the smallest comprehensive performance.

The experimental data are divided into three types: 70% of the total data are used to train the networks, 15% to validate the networks, and 15% to test the networks. The data selection of training, validation and test may be somewhat arbitrary, and these data are based on approximate uniform variation of $\mathrm{Re}_{\mathrm{Dc}}$ and total number of data. Detailed information are presented in the following section.

Table 1: Classical experiment correlations of the finned oval-tube heat exchanger

	$\theta = 90°$	$\theta = 60°$
Nu	$\mathrm{Nu} = 1.76\mathrm{Re}_{\mathrm{Dc}}^{0.42}$	$\mathrm{Nu} = 1.90\mathrm{Re}_{\mathrm{Dc}}^{0.43}$
f	$f = 78.76/\mathrm{Re}_{\mathrm{Dc}}^{0.44}$	$f = 42.46/\mathrm{Re}_{\mathrm{Dc}}^{0.37}$
	$\theta = 45°$	$\theta = 30°$
Nu	$Nu = 1.15\mathrm{Re}_{\mathrm{Dc}}^{0.48}$	$\mathrm{Nu} = 1.16\mathrm{Re}_{\mathrm{Dc}}^{0.46}$
f	$f = 47.39/\mathrm{Re}_{\mathrm{Dc}}^{0.39}$	$f = 51.97/\mathrm{Re}_{\mathrm{Dc}}^{0.39}$

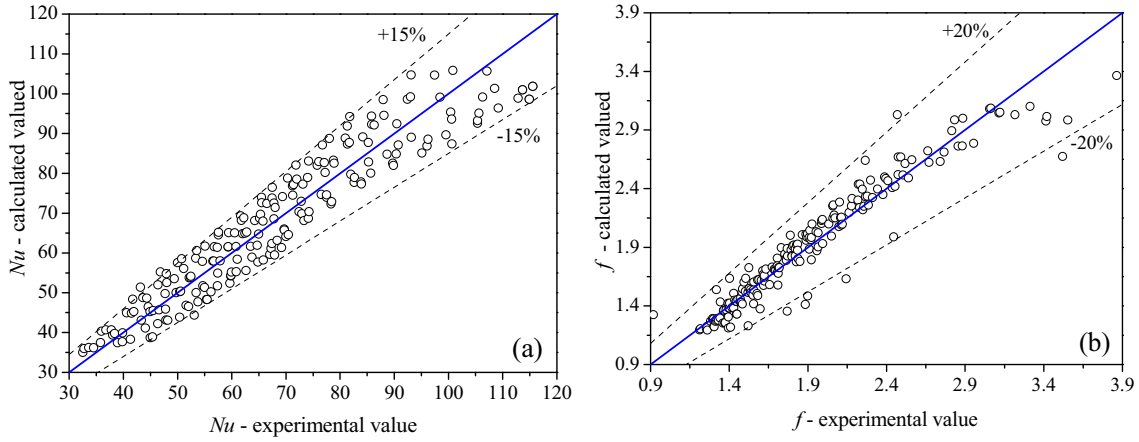

Figure 5: Comparisons of experimental value with the calculated value from correlations including angles: (a) Nu and (b) *f*.

3 Neural network configuration

ANNs consist of a great number of interconnect neurons. Figure 7 illustrates two typical full-connect network configurations. Such ANNs comprise not less than three layers with a great many nodes, which are the input layer, the hidden layer, and the output layer, and there can be more than one hidden layer to be adjusted to satisfy the desire to predict the objective parameters well. Nodes assembled together into a column are called a layer. Each connection between two nodes with a real value is called weight. A node sometimes called neuron is a basic information processing and operating unit in a neural network. For each neuron, there exists an activation and a bias associated it. The feedforward or multilayer perception neural network is widely applied in engineering applications among different types of ANNs [22]. The input information is propagated forward through the network, while the output error is back propagated through the networks for updating the weights.

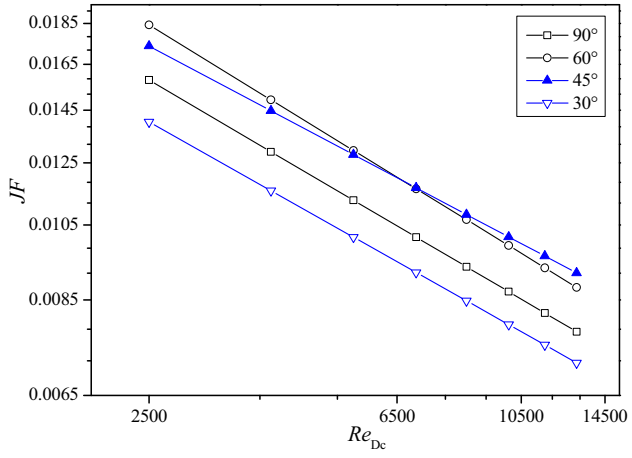

Figure 6: Comparisons of JF factors under various air inlet angles.

As described in Figure 7(a), the first layer with 10 nodes are called the input layer, and the last layer with 2 nodes are called the output layer, while the other two layers in the middle are called hidden layers. There are two hidden layers (with 10 and 5 nodes, respectively) of the configuration in Figure 7(a) called 10-8-5-2. Although there are many ways to design and implement ANN, it is difficult to find an optimal network in consideration of the uniqueness of a real problem. Therefore, a prior choice, such as selection of network topology, training algorithm, and network size, should be made on experience to keep the task to a manageable work [21,22].

Neural networks do well in fitting functions. In fact, there is a proof that a fairly simple neural network can fit any practical function. The standard network used for function fitting in the ANN fitting tool is a two-layer feedforward network trained with Levenberg–Marquardt, with a sigmoid transfer function in the hidden layer and a linear transfer function in the output layer. The default number of hidden neurons is set to 10, and it can be increased later if the network training performance is poor. The number of output neuron is determined by the target value associated with each input vector [41].

As mentioned earlier, the experimental data are partitioned into three parts: training data, validation data, and testing data during ANN training processes. Training data are presented to train the network, and the network is adjusted according to its error; validation data are used to measure the network generalization and to halt training when generalization stops improving; testing data have no influence on training and supply an independent measure of network generalization capability during and after training. Function fitting is the process of training

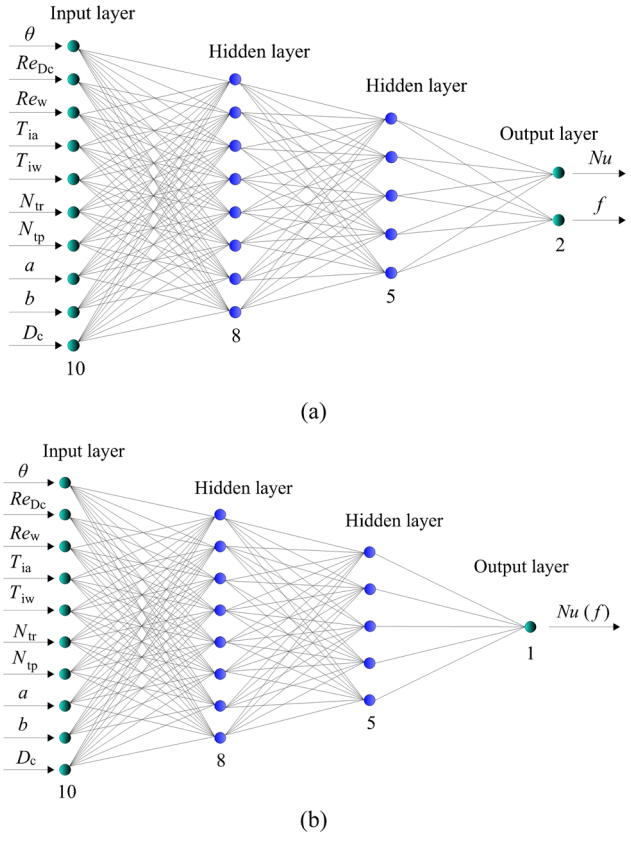

Figure 7: Configurations of two neural networks used for function fitting for a finned oval-tube heat exchanger: (a) 10-8-5-2 neural network and (b) 10-8-5-1 neural network.

a neural network on a set of inputs to produce a correlated set of target outputs. Once a neural network has fitted the data, it will produce a generalization of the input–output relationship and can be utilized to generate outputs for inputs that were not trained on.

For the tested finned oval-tube heat exchanger in this article, 10 independent parameters were fed to the input layer of the network (as shown in Figure 7): the air inlet angles (θ), the Reynolds number of the air side ($\mathrm{Re_{Dc}}$), the Reynolds number of the water side ($\mathrm{Re_w}$), the temperature of the inlet air (T_{ia}) and the inlet water (T_{iw}), the number of tube rows (N_{tr}), the number of tube-passes (N_{tp}), the outer length of the major axis (a), the outer length of the minor axis (b), and the fin collar outside diameter (D_{c}). The main reason for selection of these ten input variables is that these are the main parameters of the heat exchanger and affect the target variables. These variables are independent. The output layer contains two parameters: the Nusselt number (Nu) and the friction factor (f), which is shown in Figure 7(a). To find out the difference between the results of Nu and f predicted separately with those of Nu and f predicted together, Nu and f are also predicted severally, whose corresponding configuration of ANN is shown in Figure 7(b), called 10-8-5-1.

In the present study, the experimental data for each air inlet angle are trained separately by ANN. When Nu and f are predicted together, for 90°, the input dataset is a 10×63 matrix, representing 63 samples of 10 elements, and the output dataset is a 2×63 matrix, representing 63 samples of 2 elements; and the input datasets of other three air inlet angles (60°, 45°, and 30°) are 10×44 matrix, 10×45 matrix, and 10×45 matrix, respectively; and the output datasets are 2×44 matrix, 2×45 matrix, and 2×45 matrix, respectively. When Nu and f are predicted separately, the network configuration of 10-8-5-1 shown in Figure 7(b) is applied, and the input datasets are the same as the ones when Nu and f are predicted together, while the output datasets of the four air inlet angles (90°, 60°, 45°, and 30°) are 1×63 matrix, 1×44 matrix, 1×45 matrix, and 1×45 matrix, respectively. Besides, when the experimental data of the four air inlet angles are fitted together to predict the Nu and f together or separately, the input datasets are 10×197 matrix; and the output datasets are 2×197 matrix or 1×197 matrix, respectively.

In addition, as the physical units of the ANN input–output variables are different and the numerical ranges of the ANN input–output data are different, to eliminate these impacts, it is desirable to normalize all the input–output data with the largest and smallest values of each of the data sets. Consequently, to avoid any computational difficulty and to increase the training speed and improve the convergent behavior, all of the input–output pairs were normalized into the range of 0.15–0.85 based on the previous studies [10,21,42], within which the activation function has an appropriate gradient. That is, the input variables were scaled through the transformations:

$$x_{\mathrm{i}} = \frac{x_{\mathrm{i}} - x_{\mathrm{i,min}}}{x_{\mathrm{i,max}} - x_{\mathrm{i,min}}}(S_{\max} - S_{\min}) + S_{\min}, \tag{3}$$

where $S_{\max}$ and $S_{\min}$ are 0.85 and 0.15, respectively. $x_{\mathrm{i,max}}$ is the maximum, and $x_{\mathrm{i,min}}$ is the minimum value of the individual input variable x_{i}. So, even though the original data is composed of dimensional unit and nondimensional unit, the scaled input data are surely within the range of 0.15–0.85. Such normalization is also applied to new inputs to predict the Nusselt number and the friction factor.

4 Results

In fitting problems, the ANN function fitting can select data, create, and train a network. The mean-squared error (MSE) and regression analysis are used to evaluate the performance of ANN models. It is quantified in terms of MSE, which is the average squared difference between the outputs (the predicted data) and the targets (the actual data) according to equation (4). Lower values are better. A value closer to 0 indicates that a fit is more useful for prediction, and zero means no error. Also linear regression R measures the correlation between outputs and targets using equation (5). An R value of 1 means a close relationship and 0 means a random relationship. MSE reflects the mean accuracy of the prediction, while R reflects the scatter of the prediction. Both quantities are important for an assessment of the relative success of the ANN analysis.

$$\mathrm{MSE} = \frac{1}{n}\sum_{i=1}^{n}(E_i - P_i)^2, \tag{4}$$

$$R = \frac{\sum_{i=1}^{n}(E_i - \overline{E})(P_i - \overline{P})}{\sqrt{\sum_{i=1}^{n}(E_i - \overline{E})^2}\sqrt{\sum_{i=1}^{n}(P_i - \overline{P})^2}}, \tag{5}$$

where E is the experimental data (that is, the target value), P is the predicted value obtained from ANN (that is, the output value), and n is the total number of data. $\bar{E}$ and $\bar{P}$ are the mean values of E and P, respectively. Besides, when MSE is used to evaluate the performance of experimental correlations acquired from the traditional methods and P is the computed value obtained from the experimental correlations.

Note that in Table 2, MSE is the average squared difference, which is determined from the outputs and targets variables. Fifteen ANN configurations are trained, and the prediction performances are compared. The values of MSE of ANN are much smaller than the correlations. Through the comparisons, it can be found that the performance values (MSE) of the results obtained by different ANN configurations are very close. Considering the minimum errors of the predicting Nusselt number (Nu) and the friction factor (f), ANN configuration of 10-8-5-2 with four layers, which is shown in Table 2 with bold font, is selected to predict the heat transfer and flow resistance performances of the finned oval-tube heat exchanger in this article.

4.1 Nu and f predicted together for four different angles

As mentioned earlier, the training of the neural network was terminated when the performance measured with the validation data stops improving. Figure 8 shows the train, validation, and test performances (MSE) during the neural network training under the air inlet angle at 90° when Nu and f are predicted together. During the iterative training of a neural network, an epoch is a single pass through the entire training set. It can be seen that the mean squared error descend rapidly, and the best validation performances are acquired less than 11 epochs.

Both MSE and R are significant for an evaluation of the relative success of the ANN function fitting analysis. The performances of the function fitting with ANN for Nu and f predicted together are presented in Table 3, which also lists the values of MSE. Figure 9 depicts the linear regressions of the outputs relative to targets of ANN function fitting and also gives the values of R and the linear regression correlations of the output data comparative with the target data of training, validation, test, and all processes, under the air inlet angle $\theta = 90°$. It can be noticed that the values of R are more than 0.951, which shows that all the output data and target data have close relationships.

Besides, Table 4 presents the comparison of MSE of ANN prediction with that of the experimental correlations presented in Table 1. It can be seen that all the values of MSE of ANN function fitting are smaller than those of the correlations. That is, the results from ANN are better than the ones from the correlations.

4.2 Nu and f predicted separately for four different angles

For comparing the predicted performances with those of Nu and f predicted together, Nu and f are predicted separately, and the performances of ANN prediction are presented in Table 3. The results of Nu and f predicted together and separately are compared with those from correlations, which are presented in Table 4. It can be noticed that the values of MSE of function fitting using ANN are much smaller than those of correlations. It

means that the results from ANN function fitting are better than the ones from experimental correlations. It is indicated that in general it is useful of ANN function fitting to fit experimental data to predict unknown cases, instead of correlations.

From Table 4, it can be also seen that the values of MSE are relatively close when Nu and f are predicted separately and together. The comparative results of MSE of Nu and f predicted together and separately by ANN with those of classical correlations are shown in Figure 10. This result can be seen intuitively from the figure.

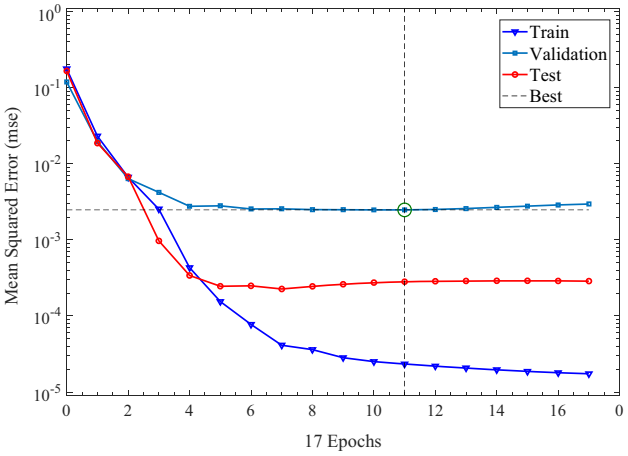

Figure 8: ANN performances of the training record at the air inlet angle $\theta = 90°$.

4.3 Nu and f predicted for the four angles

The datasets of the four air inlet angles are fitted together to predict Nu and f together or separately. The performances and comparisons when Nu and f are predicted together and presented in Table 5, while those when Nu and f are predicted separately are presented in Table 6. The comparisons of MSE of ANN with those of the correlations with air inlet angles are also presented in Tables 5 and 6. It can be seen that the values of MSE of ANN are smaller than those of correlations. Thus, it can be also thought that better results could be acquired from ANN predictions than from the experimental correlations.

From the comparisons of the performances of ANN prediction presented in Tables 5 and 6, it can be found that the values of MSE of Nu and f predicted separately are smaller than the corresponding values of MSE of Nu and f predicted together. Besides, comparing the performances of the four air inlet angles fitted together in Tables 5 and 6 with those of them fitted separately in Table 4, the latter manner have higher precisions in most cases. So it can be said that the results when the data of the four air inlet angles fitted separately are better than those when the data of the four air inlet angles fitted together through ANN approach, because the thermal performances of the four air inlet angles are distinctly different, and large errors would be brought into the predicted results if the data of the four angles are fitted together to predict Nu and f.

Table 2: Comparison of performances (MSE) by different ANN configurations with at $\theta = 90°$

Configuration	Performances of ANN				ANN		Correlations	
	All	Train	Validation	Test	Nu	f	Nu	f
10-8-2	0.0006	0.0004	0.0007	0.0013	1.30096	0.0149	6.2535	0.0227
10-7-2	0.0006	0.0007	0.0002	0.0010	1.4874	0.0165		
10-6-2	0.0003	0.0002	0.0004	0.0006	1.0114	0.0077		
10-5-2	0.0004	0.0003	0.0007	0.0004	1.2492	0.0092		
10-9-6-2	0.0004	0.0001	0.0005	0.0022	2.0759	0.0100		
10-8-6-2	0.0004	0.0005	0.0005	0.0003	1.1984	0.0114		
10-8-5-2	**0.0004**	**0.0000**	**0.0025**	**0.0003**	**0.7897**	**0.0108**		
10-8-4-2	0.0003	0.0001	0.0005	0.0016	1.6703	0.0079		
10-7-6-2	0.0009	0.0004	0.0007	0.0034	1.4683	0.0243		
10-7-5-2	0.0005	0.0001	0.008	0.0017	1.4126	0.0116		
10-7-4-2	0.0007	0.0003	0.0012	0.0021	2.3294	0.0164		
10-6-4-2	0.0004	0.0003	0.0004	0.0010	0.9583	0.0109		
10-5-4-2	0.0004	0.0002	0.0008	0.0008	1.1945	0.0096		
10-9-8-6-2	0.0005	0.0001	0.0018	0.0010	1.3562	0.0121		
10-9-7-5-2	0.0005	0.0000	0.0010	0.0026	1.2655	0.0131		

5 Discussion

Figure 10 shows the comparative results of MSE of Nu and *f* predicted together and separately by ANN with those of classical correlations. From Figure 10, it can be seen that the values of MSE of ANN prediction are all much smaller than those of the correlations, whether Nu and *f* are predicted together or separately. The comparison of MSE of Nu and *f* predicted together for the four air inlet angles with classical correlations and correlations with the air inlet angles is shown in Figure 11, from which it can be clearly seen that the values of MSE from the ANN prediction are smaller than experimental correlations, excepting the one of *f* for 60°. So it is demonstrated that ANN prediction is much effective than the experimental correlations.

In addition, the experimental data of only four air inlet angles are acquired from ref. [34–36]. So Nu and *f* under only these four angles are predicted due to lack of experimental data of other angles. However, the heat transfer performances under other angles are often expected in practical engineering applications. Thus, the heat transfer performances under different air inlet angels could be predicted if more data of other air inlet angles can be acquired through numerical simulation or other methods.

It is well known that ANN is one of computer intelligence algorithms, and there are no constant correlations to express them. This article has only studied the ANN function fitting tool to fit the experimental data to predict Nu and *f* and compared the performances of ANN with those of the experimental correlations. These processes can be used to describe and demonstrate how the experimental data are fitted through ANN approach to find out the input–output relationship to predict the unknown cases. By comparing the results, it can be concluded that the results from ANN are better than the ones from the experimental correlations. Therefore, although there is no any constant correlation for ANN, the network configuration shown in Figure 7 can be used for designers or engineers to predict the unknown cases of the finned oval-tube heat exchanger. In this article, the 10-8-5-2 neural network was trained, validated, and tested. All the parameters of the neural network including the network configuration, number of nodes, and weight coefficient of each node are recorded in the program. When it is used to predict an unknown case, the ANN program can start to run with the input data, and the expected results can be obtained.

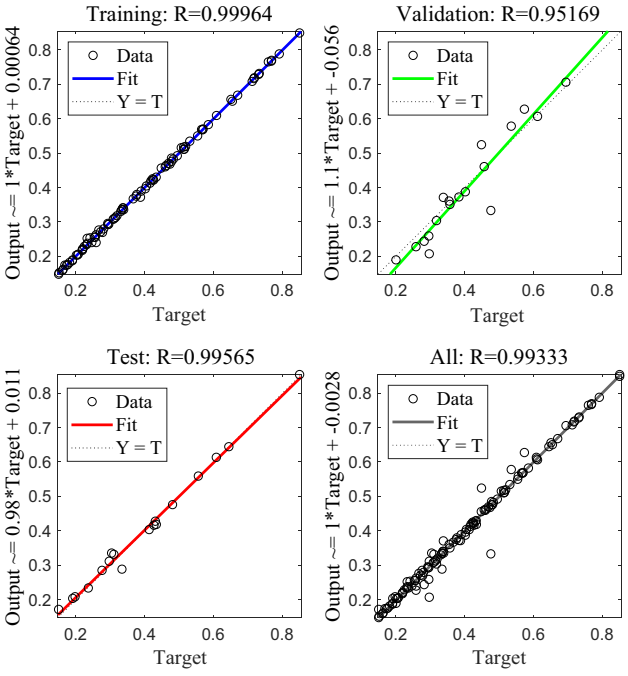

Figure 9: ANN linear regressions at the air inlet angle θ = 90°.

Moreover, the heat transfer performance prediction of heat exchangers is one of the significant objectives

Table 3: Performances of ANN prediction under four different air inlet angles

Angles/°		Nu and *f* predicted together				Nu and *f* predicted separately			
		All	Train	Validation	Test	All	Train	Validation	Test
90	Nu	0.0004	0.000	0.0025	0.0003	0.0003	0.0001	0.0016	0.0004
	f					0.0010	0.0005	0.0007	0.0034
60	Nu	0.0002	0.000	0.0014	0.001	0.0001	0.0000	0.0007	0.0004
	f					0.0005	0.0000	0.0019	0.0034
45	Nu	0.0011	0.0011	0.0039	0.0017	0.0002	0.0000	0.0005	0.0011
	f					0.0018	0.0012	0.0037	0.0029
30	Nu	0.0005	0.0001	0.0035	0.0008	0.0000	0.0000	0.0002	0.0001
	f					0.001	0.0009	0.0006	0.0017

Table 4: Comparison of MSE of ANN prediction with that of classical correlations under different angles

Angles/°	Nu and *f* predicted together		Nu and *f* predicted separately		Classical correlations	
	Nu	*f*	Nu	*f*	Nu	*f*
90	0.7897	0.0108	0.8058	0.0137	6.2535	0.0227
60	0.7179	0.0031	1.06	0.0038	8.1203	0.0128
45	1.6774	0.0216	2.3193	0.0192	8.7024	0.0399
30	0.4951	0.0111	0.2366	0.0114	2.7339	0.0178

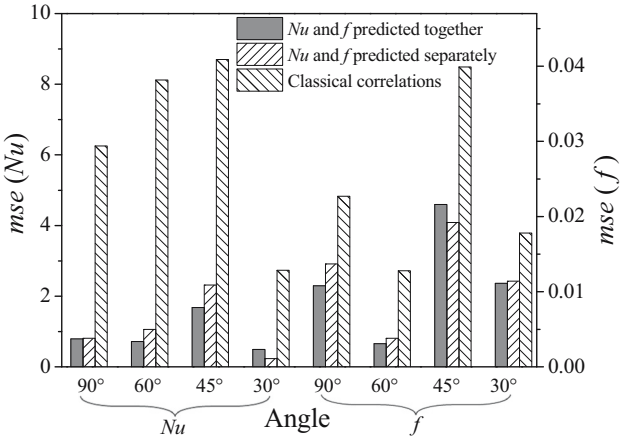

Figure 10: Comparison of Nu and *f* predicted together and separately with classical correlations.

for designers and engineers because of the limited experimental conditions. Dimensionless correlations are usually obtained according to the limited experimental data, for example, Nu vs Re and *f* vs Re, sometimes including Pr and geometric factors. It is based on some assumptions to acquire the dimensionless correlations, which would bring huge error for a real problem. As shown in the aforementioned figures and tables, the results acquired from ANN are much better than those from correlations. Better results can be obtained through ANN approach, excluding some assumptions that empirical correlations require, such as the forms of correlations, the flow patterns, and the working fluid properties. Moreover, it can be found that to predict thermal performances based on limited experimental data through the ANN approach, it not only can significantly save experimental cost but also have higher precision than experimental correlations. Therefore, we can come to the conclusion that the ANN approach is more useful and convenient than correlations for designers and engineers to predict unknown cases of a given heat exchanger, especially to model the complicated heat exchangers based on the limited experimental data in engineering applications.

6 Conclusions

In the present study, a dimensionless experimental correlation equation including air inlet angles is proposed to make the correlation have a wide range of applicability. Then thermo-hydraulic performances for the finned oval-tube heat exchanger with two rows of tubes and single tube-pass under four different air inlet angles are predicted by the ANN approach based on the limited experimental data. The performance comparisons are made between ANN with the experimental correlations, between Nu and *f* predicted separately with Nu and *f* predicted together, and between the data of the four air inlet angles fitted separately with those fitted together. Based on the aforementioned comparison results, the following conclusions are drawn.

Table 5: Performances of ANN and comparisons of MSE when Nu and *f* predicted together for the four air inlet angles

Angles/°	Performances of ANN				ANN		Classical correlations		Correlations with angles	
	All	Train	Validation	Test	Nu	*f*	Nu	*f*	Nu	*f*
90	0.0005	0.0004	0.0009	0.0005	0.8673	0.0114	6.2535	0.0227	36.99	0.0251
60					2.7824	0.0154	8.1203	0.0128		
45					2.9692	0.0163	8.7024	0.0399		
30					1.6116	0.0148	2.7339	0.0178		

Table 6: Performances of ANN and comparisons of MSE when Nu and *f* predicted separately for the four air inlet angles

	Angles/°	Performances of ANN				Comparison of MSE	
		All	Train	Validation	Test	ANN	Correlations with angles
Nu	90	0.0001	0.0000	0.0003	0.0002	0.7079	36.99
	60					2.6084	
	45					1.9378	
	30					0.4717	
f	90	0.0009	0.0006	0.0022	0.001	0.0135	0.0251
	60					0.0123	
	45					0.0269	
	30					0.0131	

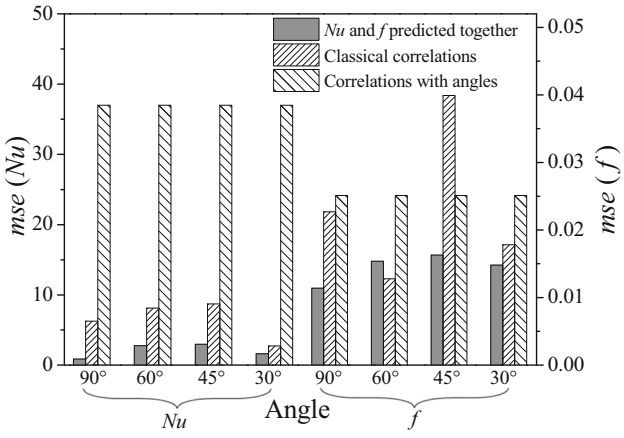

Figure 11: Comparison of Nu and *f* predicted together with classical correlations including angles.

(1) The dimensionless experimental correlation equations including air inlet angles for the Nusselt number and the flow friction factor are proposed to evaluate the performances of others angles.
(2) The data of the four air inlet angles fitted separately have higher precisions than those fitted together to predict the thermal performances in most cases.
(3) ANN prediction is superior to the experimental correlations for predicting Nusselt numbers and friction coefficients, excluding some assumptions, such as the forms of correlations, the flow patterns, and the working fluid properties. The ANN approach could be recommended to predict the thermal performances for unknown cases in a thermal system.

Acknowledgments: This work was supported by the National Natural Science Foundation of China (Grant No. 51806236), the Fundamental Research Funds for the Central Universities (Grant No. 2015XKMS059), and Foundation of Key Laboratory of Thermo-Fluid Science and Engineering (Xi'an Jiaotong University), Ministry of Education, Xi'an 710049, P. R. China (Grant No. KLTFSE2017KF01).

Conflict of interest: The authors declare no conflict of interest.

Author contributions: All parts contained in the research carried out by the authors through hard work and a review of the various references and contributions in the field of data analysis and method.

References

[1] Wang FL, Tang SZ, He YL, Kulacki FA, Yu Y. Heat transfer and fouling performance of finned tube heat exchangers: Experimentation via on line monitoring. Fuel. 2019;236:949–59.
[2] Chen HT, Hsieh YL, Chen PC, Lin YF, Liu KC. Numerical simulation of natural convection heat transfer for annular elliptical finned tube heat exchanger with experimental data. Int J Heat Mass Transf. 2018;127:541–54.
[3] Ma Y, Yuan Y, Liu Y, Hu X, Huang Y. Experimental investigation of heat transfer and pressure drop in serrated finned tube banks with staggered layouts. Appl Therm Eng. 2012;37:314–23.
[4] Srisawad K, Wongwises S. Heat transfer characteristics of a new helically coiled crimped spiral finned tube heat exchanger. Heat Mass Transf. 2009;45(4):381–91.
[5] Wang CC, Chi KY, Chang CJ. Heat transfer and friction characteristics of plain fin-and-tube heat exchangers, part ii: Correlation. Int J Heat Mass Transf. 2000;43(15):2693–700.
[6] Runge J, Zmeureanu R. Forecasting energy use in buildings using artificial neural networks: A review. Energies. 2019;12:17.
[7] Dong Z. An artificial neural network compensated output feedback power-level control for modular high temperature gas-cooled reactors. Energies. 2014;7(3):1149–70.

[8] Hosoz M, Ertunc HM, Bulgurcu H. Performance prediction of a cooling tower using artificial neural network. Energy Convers Manag. 2007;48(4):1349–59.
[9] Wang QW, Xie GN, Zeng M, Luo LQ. Prediction of heat transfer rates for shell-and-tube heat exchangers by artificial neural networks approach. J Therm Sci. 2006;15(3):257–62.
[10] Pacheco-Vega A, Sen M, Yang KT, McClain RL. Neural network analysis of fin-tube refrigerating heat exchanger with limited experimental data. Int J Heat Mass Transf. 2001;44(4):763–70.
[11] Babu BV, Munawar SA. Differential evolution strategies for optimal design of shell-and-tube heat exchangers. Chem Eng Sci. 2007;62(14):3720–39.
[12] Wang QW, Liang HX, Xie GN, Zeng M, Luo LQ, Feng ZP. Genetic algorithm optimization for primary surfaces recuperator of microturbine. J Eng Gas Turbines Power-Transactions ASME. 2007;129(2):436–42.
[13] Xie GN, Sunden B, Wang QW. Optimization of compact heat exchangers by a genetic algorithm. Appl Therm Eng. 2008;28(8):895–906.
[14] Beigzadeh R, Rahimi M, Parvizi M. Experimental study and genetic algorithm-based multi-objective optimization of thermal and flow characteristics in helically coiled tubes. Heat Mass Transf. 2013;49(9):1307–18.
[15] Han WT, Tang LH, Xie GN, Wang QW. Performance comparison of particle swarm optimization and genetic algorithm in rolling fin-tube heat exchanger optimization design. Proceedings of 2008 ASME summer heat transfer conference. Jacksonville, Florida USA; 2008, August 10-14.
[16] Ravagnani MASS, Silva AP, Biscaia EC, Caballero JA. Optimal design of shell-and-tube heat exchangers using particle swarm optimization. Ind Eng Chem Res. 2009;48(6):2927–35.
[17] Du XP, Chen GD, Zeng M, Wang QW. Design and optimization of shell-and-tube heat exchanger by goose ldw-PSO. J Eng Thermophys. 2010;31(4):679–81.
[18] Cai J. Predicting the critical heat flux in concentric-tube open thermosiphon: A method based on support vector machine optimized by chaotic particle swarm optimization algorithm. Heat Mass Transfer. 2012;48(8):1425–35.
[19] Sen M, Yang KT. Applications of artificial neural networks and genetic algorithms in thermal engineering. In: Kreith F, editor. The crc handbook of thermal engineering. Boca Raton, Florida: CRC Press; 2000.
[20] Yang KT, Sen M. Artificial neural network-based dynamic modeling thermal systems and their control. In: Wang BX, editor. Heat Transfer Science and Technology. Beijing: Higher Education Press; 2000.
[21] Xie GN, Wang QW, Zeng M, Luo LQ. Heat transfer analysis for shell-and-tube heat exchangers with experimental data by artificial neural networks approach. Appl Therm Eng. 2007;27(5–6):1096–104.
[22] Xie G, Sunden B, Wang Q, Tang L. Performance predictions of laminar and turbulent heat transfer and fluid flow of heat exchangers having large tube-diameter and large tube-row by artificial neural networks. Int J Heat Mass Transf. 2009;52(11–12):2484–97.
[23] Gao M, Sun F, Zhou S, Shi Y, Zhao Y, Wang N. Performance prediction of wet cooling tower using artificial neural network under cross-wind conditions. Int J Therm Sci. 2009;48(3):583–9.
[24] Akbari S, Hemingson HB, Beriault D, Simonson CJ, Besant RW. Application of neural networks to predict the steady state performance of a run-around membrane energy exchanger. Int J Heat Mass Transf. 2012;55(5–6):1628–41.
[25] Akbari S, Simonson CJ, Besant RW. Application of neural networks to predict the transient performance of a run-around membrane energy exchanger for yearly non-stop operation. Int J Heat Mass Transf. 2012;55(21–22):5403–16.
[26] Zdaniuk GJ, Chamra LM, Keith Walters D. Correlating heat transfer and friction in helically-finned tubes using artificial neural networks. Int J Heat Mass Transf. 2007;50(23–24):4713–23.
[27] Zdaniuk GJ, Walters DK, Luck R, Chamra LM. A comparison of artificial neural networks and symbolic-regression-based correlations for optimization of helically finned tubes in heat exchangers. J Enhanced Heat Transf. 2011;18(2):115–25.
[28] Mohanraj M, Jayaraj S, Muraleedharan C. Applications of artificial neural networks for refrigeration, air-conditioning and heat pump systems—A review. Renew Sustain Energy Rev. 2012;16(2):1340–58.
[29] Nasruddin S, Sholahudin P, Satrio P, Mahlia TMI, Giannetti N, Saito K. Optimization of hvac system energy consumption in a building using artificial neural network and multi-objective genetic algorithm. Sustain Energy Technol Assess. 2019;35:48–57.
[30] Sharifi K, Sabeti M, Rafiei M, Mohammadi AH, Ghaffari A, Asl MH, et al. A good contribution of computational fluid dynamics (CFD) and GA-ANN methods to find the best type of helical wire inserted tube in heat exchangers. Int J Therm Sci. 2020;154:106398.
[31] Garud KS, Seo J-H, Cho C-P, Lee MY. Artificial neural network and adaptive neuro-fuzzy interface system modelling to predict thermal performances of thermoelectric generator for waste heat recovery. Symmetry-Basel. 2020;12:2.
[32] Nasirzadehroshenin F, Sadeghzadeh M, Khadang A, Maddah H, Ahmadi MH, Sakhaeinia H, et al. Modeling of heat transfer performance of carbon nanotube nanofluid in a tube with fixed wall temperature by using ANN-GA. Eur Phys J Plus. 2020;135:2.
[33] Liu Z, Li H, Shi L, Zhang Y. Numerical study of the air inlet angle influence on the air-side performance of plate-fin heat exchangers. Appl Therm Eng. 2015;89:356–64.
[34] Du XP, Zeng M, Wang QW, Dong ZY. Experimental investigation of heat transfer and resistance characteristics of a finned oval-tube heat exchanger with different air inlet angles. Heat Transf Eng. 2014;35(6–8):703–10.
[35] Du XP, Zeng M, Dong ZY, Wang QW. Experimental study of the effect of air inlet angle on the air-side performance for cross-flow finned oval-tube heat exchangers. Exp Therm Fluid Sci. 2014;52:146–55.
[36] Du XP, Yin YT, Zeng M, Yu PQ, Wang QW, Dong ZY, et al. An experimental investigation on air-side performances of finned tube heat exchangers for indirect air-cooling tower. Therm Sci. 2014;18(3):863–74.
[37] Peng H, Ling X. Neural networks analysis of thermal characteristics on plate-fin heat exchangers with limited experimental data. Appl Therm Eng. 2009; 29(11–12):2251–6.
[38] Erek A, Özerdem B, Bilir L, İlken Z. Effect of geometrical parameters on heat transfer and pressure drop characteristics of plate fin and tube heat exchangers. Appl Therm Eng. 2005;25(14–15):2421–31.

[39] Kim NH, Ham JH, Cho JP. Experimental investigation on the airside performance of fin-and-tube heat exchangers having herringbone wave fins and proposal of a new heat transfer and pressure drop correlation. J Mech Sci Technol. 2008;22(3):545–55.
[40] Yun JY, Lee KS. Influence of design parameters on the heat transfer and flow friction characteristics of the heat exchanger with slit fins. Int J Heat Mass Transf. 2000;43(14):2529–39.
[41] Beale MH, Hagan MT, Demuth HB. Neural network toolbox™ user's guide. Natick, Massachusetts: The MathWorks, Inc.; 2012.
[42] Díaz G, Sen M, Yang KT, McClain RL. Dynamic prediction and control of heat exchangers using artificial neural networks. Int J Heat Mass Transf. 2001;44(9):1671–9.